Theory of epithelial elasticity

Matej Krajnc[1,*] and Primož Ziherl[1,2]
[1]*Jožef Stefan Institute, Jamova 39, SI-1000 Ljubljana, Slovenia*
[2]*Faculty of Mathematics and Physics, University of Ljubljana, Jadranska 19, SI-1000 Ljubljana, Slovenia*
(Received 31 August 2015; published 11 November 2015)

We propose an elastic theory of epithelial monolayers based on a two-dimensional discrete model of dropletlike cells characterized by differential surface tensions of their apical, basal, and lateral sides. We show that the effective tissue bending modulus depends on the apicobasal differential tension and changes sign at the transition from the flat to the fold morphology. We discuss three mechanisms that stabilize the finite-wavelength fold structures: Physical constraint on cell geometry, hard-core interaction between non-neighboring cells, and bending elasticity of the basement membrane. We show that the thickness of the monolayer changes along the waveform and thus needs to be considered as a variable rather than a parameter. Next we show that the coupling between the curvature and the thickness is governed by the apicobasal polarity and that the amplitude of thickness modulation along the waveform is proportional to the apicobasal differential tension. This suggests that intracellular stresses can be measured indirectly by observing easily measurable morphometric parameters. We also study the mechanics of three-dimensional structures with cylindrical symmetry.

DOI: 10.1103/PhysRevE.92.052713 PACS number(s): 87.17.Pq, 87.17.Rt, 87.19.rd

I. INTRODUCTION

A flexible rod buckles when the lengthwise compressive force exceeds a certain threshold [1]. This fundamental principle is known as the buckling instability and is very common in everyday life. The shape of the bent rod obeys the solution of Euler's elastica problem, studied around 300 years ago by James Bernoulli and Leonhard Euler [2]. Similar behavior is seen in many other physical systems. For example, a thin compressed elastic sheet either floating on the liquid surface or attached to the elastic substrate forms a single fold or various types of wrinkles [3–7]. In plants, the edge of a leaf is often wavy due to the differential growth between the edge itself and the bulk of the leaf [8,9]; wrinkles can be induced by bunching up the skin on the back of a hand [10]; cerebral cortex in human brain forms a very complex morphology [11,12]; and a variety of different morphological structures can be found in other types of animal tissues such as epithelia.

The mechanics of modulated epithelial structures has been theoretically studied using two different hypotheses: (i) buckling due to area mismatch between the tissue and the underlying substrate [13–15] and (ii) folding due to intraepithelium stresses generated by the actomyosin cortex [16–19]. The former scenario has been explored within the classical theory of elasticity of homogeneous solid plates [1]. Here epithelial folding is induced by the growth of the tissue and a variety of complex three-dimensional (3D) morphologies have been obtained. Within the second scenario, cells are treated as incompressible droplets characterized by differential surface tensions of the functionally distinct cell sides [20]. By now, mostly solutions describing epithelial folds have been studied [16–18] and therefore many questions regarding the 3D generalization and the effective elasticity of the model tissue remain unanswered. The thusly obtained shapes of folds are very smooth, which suggests that an effective elastic theory for this kind of mechanics could be derived, allowing one to deal with some of the open issues. Recently, a similar approach has been used to derive a continuum model of the out-of-plane deformations in a 2D tiling formed by the apical faces of cells in the epithelium [21].

A continuum theory based on the discrete model of epithelial cells seems the most straightforward way to quantitatively describe how the mechanics on the subcellular level affects the features of the tissue; for example, to quantify cell height modulation along the waveform and the groove-crest asymmetry as well as to explain what type of elasticity is associated with stresses due to apicobasal differential tension and how the spontaneous folding is driven. Moreover, from the perspective of numerical methods a continuum theory may be technically easier to solve, especially in 3D, where it disposes of the problem of the tissue in-plane topology [22,23] which is expected to have a subdominant effect on the equilibrium tissue shape.

In this paper, we derive the effective energy functional that describes a 2D cross section of the epithelium. We find that the tissue bending modulus depends on the apicobasal differential tension and can be either positive or negative. Next, we analytically study the coupling between tissue thickness and curvature and we show how thickness modulation along the waveform depends on apicobasal differential tension. Furthermore, we show that a finite-wavelength structures of the tissue with negative bending modulus can be stabilized by the local geometry of cells or their impenetrability or by the elasticity of the basement membrane. Apart from the simplified 2D version of the model, we also study 3D structures with cylindrical symmetry where certain effects not present in the 2D model are included.

II. THE MODEL

Our theoretical model is based on the differential adhesion hypothesis [20] and describes a single layer of incompressible epithelial cells. Their energy is associated with the surface tension in actomyosin cortical network, the differential surface tension due to apicobasal polarity, and the negative surface

*matej.krajnc@ijs.si

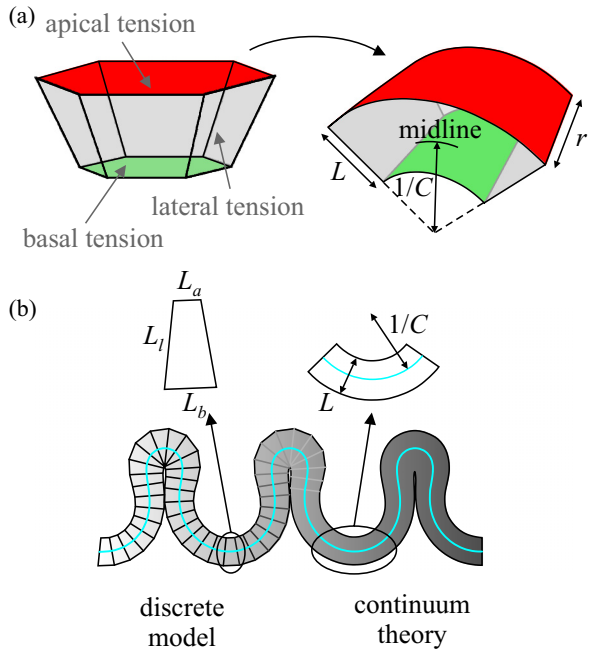

FIG. 1. (Color online) Schematic of the model epithelial cell characterized by different surface tensions on apical, basal, and lateral sides [(a), left]. The right panel shows a bent segment of tissue parametrized by midline curvature C, epithelial thickness L, and depth r. In the discrete representation this body can be treated as the model cell. Schematic cross section of three epithelial waveforms in the discrete representation (b), parametrized by cell side lengths (L_a, L_b, and L_l) and the continuous waveform, parametrized by the midline local curvature C and local tissue thickness L. Gray shading denotes the transition from the discrete to the continuum description.

tension due to cell-cell adhesion [24]. The effective surface tensions of apical, basal, and lateral cell sides Γ_a, Γ_b, and Γ_l, respectively, are introduced [Fig. 1(a)] such that the total cell energy reads

$$W = \Gamma_a A_a + \Gamma_b A_b + \frac{\Gamma_l}{2} A_l, \tag{1}$$

where A_a, A_b, and A_l are surface areas of apical, basal, and lateral cell sides, respectively.

In the special case of epithelial structures with cylindrical symmetry the model can be simplified; here "cylindrical" is used in the broad sense, describing a ruled surface defined by a single-parameter family of parallel lines. Additionally, if cells are very elongated in the direction of zero curvature the energy contribution of the front and the back lateral sides [Fig. 1(a)] may be neglected since their surface area is negligible in comparison to other cell sides. In this case the total cell energy is proportional to the cell depth (the dimension in the zero-curvature direction) r and can be rescaled as $W/r \to W = \Gamma_a L_a + \Gamma_b L_b + (\Gamma_l/2) L_l$, where L_a, L_b, and L_l are lengths of apical, basal, and lateral sides of cell cross section, respectively. This yields a simplified 2D model of epithelial cells with fixed cross section area ($A_c = \text{const}$).

Since cells' apical and basal sides are usually isometric, the above simplification might not be completely justified. Yet it turns out most features, especially those related to the differential apicobasal mechanics leading to epithelial bending, are captured within the reduced-dimensionality model. We show this in Sec. III and for completeness we then consider certain 3D effects in Sec. IV.

III. 2D CONTINUUM THEORY

Given the smoothness of the solutions obtained within the discrete model [16–18] we now derive the continuum version of the model, a theory that describes an epithelium with a given cross-section area using only tissue-scale variables: The midline curvature C and the monolayer thickness L [Fig. 1(b)].

The effective elastic energy functional is obtained by parametrizing the tissue by C and L and calculating the total energy. The contribution of apical and basal sides to the total energy is $\Gamma_a L_a + \Gamma_b L_b$, whereas evaluation of energy of the lateral sides is more demanding. Their total length depends on local curvature, local thickness, and effective area of cell cross section A_c [17], which we take into account by introducing the lateral tension density $d\Gamma_l/dA$ such that the energy of the tissue with cross-section area ΔA reads $\Delta W = \Gamma_a L_a + \Gamma_b L_b + (d\Gamma_l/dA)\Delta A L$. Here $L_a = (1 + CL/2)\Delta A/L$ and $L_b = (1 - CL/2)\Delta A/L$ are the lengths of the apical and the basal sides, respectively. The lateral tension density then can be derived from the comparison between the discrete and the continuum version of energy and reads $d\Gamma_l/dA = (\Gamma_l/A_c)\sqrt{1 + (CA_c/2L)^2}$ (Appendix A). In a flat tissue where $C = 0$, the length of the lateral cell side is L so the lateral tension density reduces to Γ_l/A_c and does not depend on the position along a waveform, whereas in a bent tissue where $C \neq 0$, the lateral tension density increases with local curvature and is larger than in the flat tissue.

The continuum version of the energy is obtained in the limit $\Delta A \to 0$ (Appendix A). It has been previously shown that in our surface tension model, folds are stable only if the magnitude of the differential apicobasal tension $|\Gamma_a - \Gamma_b|$ is large enough compared to Γ_l [18]. A large differential apicobasal tension necessitates that either Γ_a or Γ_b must be large itself because within our model, cell shape is well defined only if all three surface tensions are positive [25]. In turn, this means that $\Gamma_a + \Gamma_b \gg \Gamma_l$, too, which implies that folded epithelia are possible only in columnar epithelia where cells are tall rather than flattened. We therefore restrict the discussion to this regime where $\alpha + \beta \gg 1$ and $(CA_c/2L)^2 \ll 1$. In this case, the nondimensional energy per unit length in the first-order approximation reads

$$\frac{dw}{ds} = \alpha + \beta + \frac{\alpha - \beta}{2} cl + l^2 + \frac{1}{8} c^2, \tag{2}$$

where $\alpha = \Gamma_a/\Gamma_l$ and $\beta = \Gamma_b/\Gamma_l$ are the reduced apical and basal tension, respectively; c is the reduced midline curvature measured in units of $1/\sqrt{A_c}$ and l is the reduced epithelial thickness measured in units of $\sqrt{A_c}$. The energy w is measured in units of $\Gamma_l\sqrt{A_c}$.

The effective tissue elasticity [Eq. (2)] is based on the geometry of 2D cell cross sections with fixed area and can be interpreted by examining the four energy terms: (i) $\alpha + \beta$ corresponds to the apicobasal surface energy of the flat tissue; correction due to the curvature is taken into account by (ii) the coupling term $(\alpha - \beta)lc/2$; (iii) the stretching energy

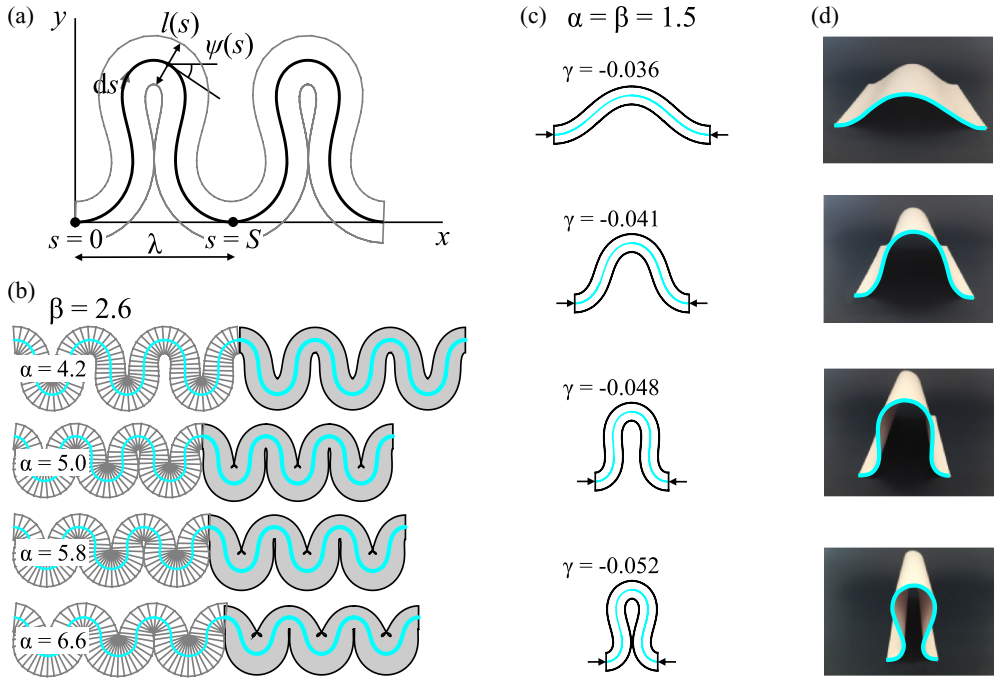

FIG. 2. (Color online) Parametrization of tissue cross-section by the angle $\psi(s)$ and tissue thickness $l(s)$ (a). In a single waveform of wavelength λ, the arc length s goes from $s = 0$ to $s = S$. A comparison between minimal-energy shapes obtained by the discrete model [17] and minimal-energy shapes computed by minimizing the elastic functional [Eq. (2)] at $\beta = 2.6$ for $\alpha = 4.2$, 5.0, 5.8, and 6.6 (b). Continuum-theory waveforms are computed at the same wavelength and number of cells per waveform as in the discrete model. Minimal-energy shapes of a segment of epithelium at $\alpha = \beta = 1.5$ for different values of compressive force $\gamma = -0.036$, -0.041, -0.048, and -0.052; γ is defined in Sec. III A (c). Equilibrium shapes of a piece of paper attached to a flat surface, the opposite ends being fixed at the distances shorter than the length of the paper (d). Thick cyan (light gray) line is added to highlight the contour. The equilibrium states of the folds correspond to the same family of curves as that of the tissue midline in panel (c).

l^2 is the energy of lateral cell sides as if the tissue were flat; and correction due to the curvature is taken into account by (iv) the bending term $c^2/8$.

Viewed as a Taylor series in c and l, the elastic theory of the model epithelium is similar to that of solid plates or thin lipid bilayers for deformations with zero Gaussian curvature [26]. The lengthening of lateral cell sides due to bending is penalized by the bending elasticity term c^2. This is similar to a lipid bilayer where bending affects the distance between the polar heads which is also penalized by the bending energy c^2 [or $(c - c_0)^2$ if the bilayer has a spontaneous curvature c_0]. In epithelia the linear term in c is multiplied by l, which here is a variable. This shows that the apicobasal polarity does not result in a spontaneous curvature as one may anticipate but instead results in the simplest possible coupling between curvature and epithelial thickness [cl term in Eq. (2)]. This term is expected to be crucial for the spontaneous epithelial folding since it introduces an asymmetry between the positively curved section and the negatively curved section of a waveform. There is no such asymmetry if the thickness is constant along the tissue which happens if the differential tension $\alpha - \beta = 0$. In this case the cl coupling vanishes and the energy simplifies to the pure bending energy $dw/ds = \text{const} + c^2/8$. Such an epithelium cannot buckle unless an external compression is applied [2,27]. Finally, in the flat epithelium ($c = 0$) $dw/ds = \alpha + \beta + l^2$, which yields the equilibrium epithelial thickness

$$l_0 = \sqrt{\alpha + \beta}\,. \tag{3}$$

This result can be viewed as the zero-order approximation in the differential tension $\alpha - \beta$.

A. Longitudinal folds: The Lagrangian

Here we study the morphology of longitudinal epithelial folds. Such shapes have a cylindrical symmetry [26] and their shape can be described by studying tissue cross section in the plane perpendicular to the folds. The shape of the tissue cross-section midline can be parametrized by the angle $\psi(s)$ between the local tangent to the midline and the horizontal axis [Fig. 2(a)]. The transformation from the Cartesian coordinates (x, y) to the $\psi(s)$ parametrization is given by $\dot{x} = \cos\psi(s)$ and $\dot{y} = -\sin\psi(s)$. In this parametrization the Lagrangian $\mathcal{L}$ reads

$$\mathcal{L} = \alpha + \beta + \frac{\alpha - \beta}{2}\dot{\psi} l + l^2 + \frac{1}{8}\dot{\psi}^2 + \mu l + \gamma(s)(\dot{x} - \cos\psi) + \eta(s)(\dot{y} + \sin\psi), \tag{4}$$

where μ, $\gamma(s)$, and $\eta(s)$ are Lagrange multipliers; μ is measured in units of $\Gamma_l/\sqrt{A_c}$, whereas γ and η are measured in units of Γ_l.

We look for equilibrium states by minimizing the action $\mathcal{S} = \int_0^S \mathcal{L}(\psi, l, \dot{\psi}, \dot{x}, \dot{y})ds$ subject to the incompressibility constraint $\int_0^S l ds = A$, where A is the cross-section area of a single waveform. In nondimensional units A is equivalent to the number of cells per waveform N in the discrete representation. The Euler-Lagrange equation for curvature $\dot{\psi}$ reduces to the

well-known Euler's elastica equation [2,27,28]

$$\ddot{\psi} + \frac{8\gamma}{(\alpha-\beta)^2-2}\sin\psi = 0. \tag{5}$$

The boundary conditions at one end of integration interval are $\psi(0) = 0$, $x(0) = x_0$, and $y(0) = y_0$, whereas the Lagrange multiplier γ needs to be varied together with $\dot{\psi}(0)$ to satisfy boundary conditions at the other end, which read $\psi(S) = 0$ and $x(S) = x_0 + \lambda$. Thus γ has the role of the force acting on a piece of tissue in the x direction to keep boundaries fixed at the distance λ [4]. Since the Lagrangian does not depend explicitly on x and y, the choice of x_0 and y_0 is arbitrary; we set $x_0 = y_0 = 0$ [Fig. 2(a)]. The integration interval S has to be varied as well to satisfy the additional boundary condition $\dot{\psi}(S) = \pm 8\sqrt{\alpha+\beta-(A/S)^2-\gamma}/\sqrt{2-(\alpha-\beta)^2}$, which is derived from the minimization of the Hamiltonian introduced in Appendix B with respect to S and is the special case of transversality condition (Appendix B and Refs. [29,30]).

B. Thickness modulation

Once the solution $\psi(s)$ is found, tissue thickness $l(s)$ can be calculated straightforwardly (Appendix B):

$$l(s) = l_0 - \frac{\alpha-\beta}{4}\dot{\psi}(s), \tag{6}$$

where $l_0 = A/S \approx \sqrt{\alpha+\beta}$ [Eq. (3)]. The thickness modulation $(\alpha-\beta)\dot{\psi}/4$ is proportional to the curvature modulation along the waveform as well as to the differential tension $\alpha-\beta$. This result confirms that intraepithelial forces resulting from apicobasal cell polarity can be measured indirectly by measuring thickness modulation and curvature profile along the fold [18]. Note that the fixed cross-section area constraint $\int_0^S l ds = A$ is satisfied automatically, since $\dot{\psi}$ averaged over one waveform is zero [31].

Equation (6) is not too surprising because the energy term that describes coupling between c and l is simply their product [Eq. (2)]. Furthermore, the elastic modulus corresponding to the coupling term is proportional to $|\alpha-\beta|$, which suggests that in the absence of apicobasal differential tension the thickness modulation vanishes. This is true only in the first-order approximation in $(c/2l)^2$ [Eq. (2)], whereas the higher-order terms including the second-order term $c^4/(128l^2)$ describe a much less trivial $c-l$ coupling even at vanishing differential tension $\alpha-\beta=0$. By treating this term perturbatively, we find that for $\alpha-\beta=0$ the thickness profile reads $l(s) = l_0 + \dot{\psi}(s)^4/(128l_0^3)$ (Appendix C). However, for values of model parameters considered here the magnitude of thickness modulation $|\dot{\psi}(s)^4/(128l_0^3)|$ is negligible and is thus not further explored.

Figure 2(b) shows the results of our continuum theory for a fixed $\beta = 2.6$ and different values of α. Apart from the shape itself, each epithelial structure is characterized by an optimal wavelength λ and an optimal number of cells per waveform N. As neither of them is known *a priori*, λ and N must be be computed by minimizing the energy with respect to both. Here we use the optimal values obtained within the discrete model (see Fig. 4 in Ref. [17]) as inputs and optimize only the tissue contour and thickness profiles. Figure 2(b) shows an almost perfect agreement of the discrete model and the continuum theory. This confirms that the mechanics of minimal-energy epithelial structures can indeed be described by the effective elasticity theory proposed here.

In absence of apicobasal differential tension ($\alpha-\beta=0$) the fold morphology is not preferred. In fact, due to vanishing coupling term, Eq. (2) reduces to the pure 2D bending energy $dw/ds = \text{const} + c^2/8$. Such a tissue buckles under external compressive force γ [Fig. 2(c)] and the midline shape corresponds to the shape of a piece of paper lying on a flat surface with opposite ends being kept at a distance smaller than the paper length [Fig. 2(d)]. This result suggests that the mechanics of our model epithelium is rather standard except for the cl coupling due to differential apicobasal tension which distinguishes the epithelial elasticity from Euler's elastica. This implies that it is precisely the cl coupling that induces spontaneous buckling of the epithelial sheet via thickness modulation as elaborated in Sec. III C.

C. Spontaneous folding: Flat-to-fold transition

Each waveform consists of a positive-curvature section (the crest) and of a negative-curvature section (the groove). If $\alpha-\beta>0$, then the groove is energetically favorable because it consists of cells with the apical side being shorter than the basal side. If $\alpha-\beta<0$, then it is exactly the opposite: The crest is energetically favorable. Tissue thickness is always increased in the energetically favorable section and decreased in the energetically unfavorable section [Eq. (6)]. Thus, due to their incompressibility the local number density of cells is also affected by the thickness modulation so the cells in favorable bend are packed more densely than in unfavorable bend. The resulting asymmetry between the groove and the crest prefers the fold morphology over the flat morphology. Despite this nontrivial mechanism, according to Eq. (5), the mechanics of our model system is formally equivalent to the folding of uniaxially compressed flexible rod [27] or a piece of paper [Fig. 2(d)]. This is surprising since the Euler's elastica does not possess this asymmetry and cannot spontaneously fold. The equivalence holds generally even if $\alpha-\beta\neq 0$.

The reason for spontaneous folding of epithelial monolayer lies in its effective bending modulus which can be obtained by comparing Eq. (5) with Euler's elastica equation [27] and reads

$$k_e = -\frac{(\alpha-\beta)^2-2}{8}. \tag{7}$$

where k_e can be either positive or negative, depending on the value of differential tension $\alpha-\beta$: A negative bending modulus prefers the fold morphology and a positive bending modulus prefers the flat morphology. Thus the effective elastic functional of the system is simply $dw/ds = \text{const} + (k_e/2)c^2$ and the energy difference between flat and folded tissue reads

$$w - w_{\text{flat}} = \frac{k_e}{2}\int_0^S c^2 ds. \tag{8}$$

The critical differential tension for the flat-fold transition $(\alpha-\beta)_c = \sqrt{2}$ [Eq. (7) and Fig. 3], which has already been predicted by the discrete model [16–18].

Figure 3 shows the force γ exerted on the piece of tissue by keeping the distance between ends fixed and varying the

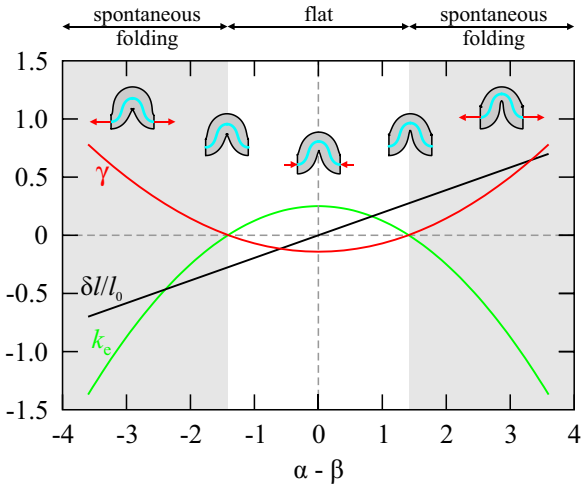

FIG. 3. (Color online) Force exerted on a segment of tissue with cross-section area $A = 25$ and $\alpha + \beta = 6.8$, fixed at $\lambda = 6$, as a function of apicobasal differential tension $\alpha - \beta$ [red (dark gray) curve]. Also included are the bending modulus k_e [green (light gray) curve] and the amplitude of tissue thickness modulation $\delta l/l_0$ (black line). At $|\alpha - \beta| = \sqrt{2}$ both γ and k_e change sign and for $|\alpha - \beta| > \sqrt{2}$ (shaded region) fold morphologies are energetically favorable over the flat state. Insets are equilibrium shapes at fixed $\lambda = 6$ and $\alpha + \beta = 6.8$ for $\alpha - \beta = -2.8, -\sqrt{2}, 0, \sqrt{2}$, and 2.8 (left to right).

differential tension $\alpha - \beta$ (red curve). The force is negative for $-\sqrt{2} < \alpha - \beta < \sqrt{2}$ where the bending modulus k_e is positive (green curve), meaning that for these values of parameter $\alpha - \beta$ the tissue is compressed. On the other hand, if $|\alpha - \beta| > \sqrt{2}$ the tissue spontaneously buckles due to internal stresses produced by apicobasal polarity. Here the force is positive and the bending modulus is negative (Fig. 3). Tissue thickness modulation is a linear function of $\alpha - \beta$ as predicted by Eq. (6) (black line in Fig. 3).

D. Stabilization of finite-wavelength folds

Even though the continuum theory predicts a spontaneous folding of the flat epithelium at $|\alpha - \beta| > \sqrt{2}$, the discrete model shows that both equilibrium wavelength and optimal number of cells per waveform are well-defined quantities (Fig. 4 in Ref. [17]). The reason for this is in two mechanisms not included in the continuum theory but accounted for by the discrete model: (i) The physical constraint of local geometry of cells and (ii) the hard-core repulsion between non-neighbouring cells.

First, in the discrete representation each cell is subject to the physical constraint of non-negative cell edge lengths. At fixed wavelength the total energy of the structure in which at least a few cells hit this constraint and have to be spatially rearranged [Figs. 4(a) and 4(b)] is larger than the total energy of the optimally shaped continuous model epithelium without cell rearrangement [Eq. (2), Fig. 2(b), and Figs. 4(a) and 4(b)]. The epithelial structure is therefore stabilized at a finite wavelength and number of cells per waveform. This constraint is not implemented in the continuum version of the model and therefore in some solutions the apical or the basal surface

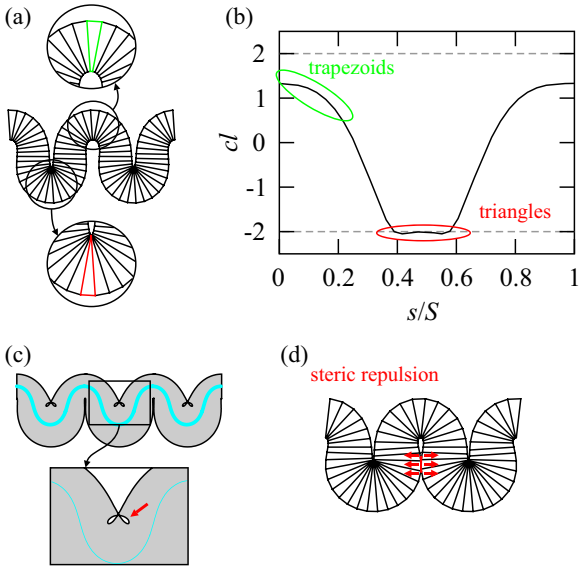

FIG. 4. (Color online) Minimal-energy shape of the tissue cross section for $\alpha = 4.2$ and $\beta = 2.6$ obtained by the discrete model (a). In this case the groove is energetically favorable over the crest and contains tall triangular cells, whereas the crest consists of trapezoidal cells. The product of curvature and thickness cl along the waveform shown in panel (b) is bounded between -2 and 2 which are the values corresponding to basally constricted cell and apically constricted cell, respectively. Minimal-energy shape of the tissue cross section for $\alpha = 6.6$ and $\beta = 2.6$ obtained by the continuum version of our model (c). The apical side of the groove makes self-intersection loops in absence of the physical constraint of positive cell side lengths. Minimal-energy shape of the tissue cross section for $\alpha = 5$ and $\beta = 2.6$ obtained by the discrete model (d). Steric repulsion acts at points where non-neighboring cells touch [red (dark gray) arrows].

self-intersect [Fig. 4(c)]. This happens as soon as locally $|cl| > 2$. We discuss this in more detail in Sec. III E. Second, tissue collapse is also prevented by steric repulsion between non-neighboring cells [Fig. 4(d)].

E. Basement membrane

Understanding the tissue mechanics based exclusively on intracellular tensions is important, one reason being that during early embryonic development of an animal the elastic substrate to which cells could be attached is not developed yet and thus cannot be involved in the morphogenetic transformations of the epithelium. Theories based solely on elastic interactions between epithelium and underlying layers therefore fall short of explaining all morphogenetic processes. However, in fully developed animals epithelial cells are attached to the basement membrane which needs to be taken into account here to extend the biological relevance of our model. This has already been done within the discrete model [18] showing that the basement membrane affects the transition from flat to fold tissue and that the wavelength of epithelial folds increases with the rigidity of the basement membrane.

The basement membrane can be modelled as a thin elastic plate with bending modulus K_{bm} [1] attached to the epithelial monolayer. In 2D the bending energy of the basement membrane reads $w_{\mathrm{bm}} = (\kappa/2)\int_{\mathrm{basal}} c_{\mathrm{bm}}^2 ds$, where

$\kappa = K_{\rm bm}/(\Gamma_l A_c)$ is its nondimensional bending modulus and $c_{\rm bm} = c/(1 - cl/2)$ is its local curvature which differs from the midline curvature c due to finite thickness of the epithelium (Appendix D). The integral of basement membrane bending energy per unit length over the basal surface can be recast as an integral over the epithelial midline:

$$w_{\rm bm} = \frac{\kappa}{2}\int_0^S \frac{c^2}{1 - lc/2} ds \tag{9}$$

and describes the interaction energy between the spontaneously folded epithelium and the membrane which prefers a flat state. The energy $w_{\rm bm}$ diverges at $lc = 2$, which happens when the tissue is folded so much that some cells become basally constricted. This indicates that the bending rigidity of the membrane could provide another mechanism stabilizing the folds at a finite wavelength.

Now we examine how the basement membrane affects the flat-to-fold transition. The stability of the flat tissue can be studied in the limit of small curvatures ($c \approx 0$), where the total energy reduces to the bending energy and the effective bending modulus of the system reads $k_{\rm eff} = k_e + \kappa$. The flat tissue is stable if $k_{\rm eff} > 0$ and unstable if $k_{\rm eff} < 0$ [Eq. (8)]. This gives the condition for minimal apicobasal differential tension needed for epithelium to form folds:

$$\alpha - \beta > \sqrt{2(1 + 4\kappa)}. \tag{10}$$

This result agrees very well with the line of flat-to-fold transition, qualitatively determined using the discrete model [18] where, on approaching the transition, the computation turned out to be very demanding due to an increasing number of cells per waveform and therefore the transition itself was estimated only roughly.

However, epithelial folds are stabilized at radia of curvature comparable to the typical cell length scale and therefore the limit of small curvatures does not apply near the equilibrium wavelength. To study the mechanics close to equilibrium we approximate the waveform by a combination of a positively curved semicircle and a negatively curved semicircle, both having the same magnitude of curvature [Fig. 5(a)]. The energy difference between this model fold state and the flat state is given by

$$w - w_{\rm flat} = w_e + w_{\rm bm}, \tag{11}$$

where $w_e = k_e c^2(\pi/c)$ is the bending energy of epithelial monolayer and $w_{\rm bm} = \kappa c^2\{1/[2 - l(c)c] + 1/[2 + l(-c)c]\}(\pi/c)$ is the bending energy of the basement membrane. Assuming that κ is small enough so as to not affect the thickness modulation, we can take $l(c) \approx l_0 - (\alpha - \beta)c/4$ [Eq. (6)]. This result is valid at deformations where the radius of curvature of the membrane is large enough compared to its thickness so the membrane bending energy can be described by Eq. (9). At very large curvatures, e.g., close to $cl = 2$ where $w_{\rm bm}$ diverges, this model of membrane elasticity is no longer physically plausible. Nonetheless, in the limit $\kappa \to 0$ it can still be used as a mathematical device accounting for the constraint on cell geometry discussed in Sec. III D without penalizing a small or moderate bending of the basal surface. The same can be done for apical cell sides by adding the energy penalty $w_{\rm a} = \kappa' c^2\{1/[2 + l(c)c] + 1/[2 - l(-c)c]\}(\pi/c)$ to the total

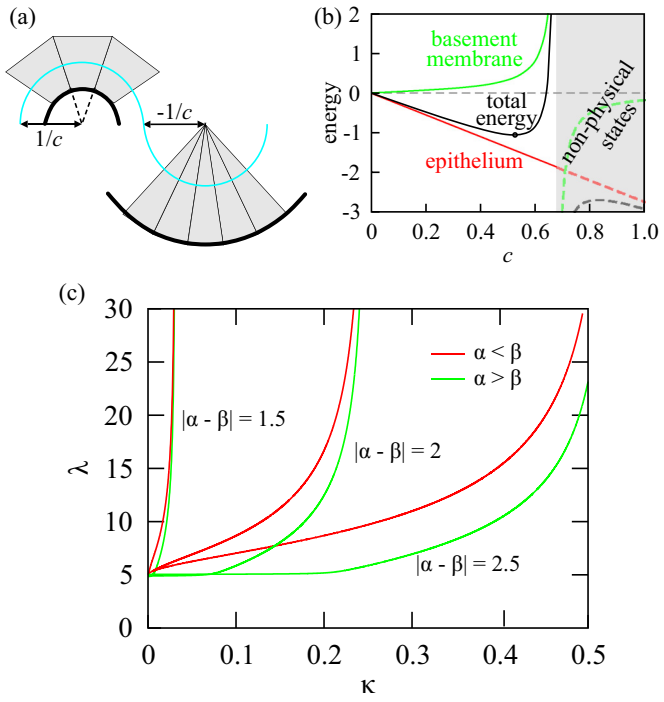

FIG. 5. (Color online) Schematic of the model waveform (a). The groove is characterized by a negative curvature $-c$ and tall triangular cells, whereas the crest has opposite curvature c and consists of trapezoidal cells. Curvature of the basement membrane is larger in the crest, where cells' basal sides are shorter than their apical sides. Energy terms w_e, $w_{\rm bm}$, and their sum $w_e + w_{\rm bm}$ at $\alpha + \beta = 6$, $\alpha - \beta = -3$, and $\kappa = 0.1$ (b). Equilibrium wavelength as a function of κ at $\alpha + \beta = 4$ for different values of differential tension $|\alpha - \beta| = 1.5$, 2, and 2.5 (c). Red (dark gray) curves correspond to the $\alpha < \beta$ case, whereas green (light gray) curves correspond to the $\alpha > \beta$ case.

energy [Eq. (11)], where $\kappa' \to 0$ corresponds to the virtual bending rigidity of the apical side of the tissue.

The monolayer bending energy w_e is a linear function of c with the slope proportional to the bending modulus $k_{\rm e}$ and thus prefers infinite c if k_e is negative [red line in Fig. 5(b)]. On the other hand, the basement membrane energy $c_{\rm bm}$ is an increasing function of c in the region of physically possible states and diverges at a finite c [green curve in Fig. 5(b)]. The sum of both energies is the total energy which has a negative value of the local minimum at finite c as long as the parameters satisfy Eq. (10) [black curve in Fig. 5(b)].

Figure 5(c) shows the equilibrium wavelength $\lambda = 4/c$ of the tissue as a function of κ for different values of $\alpha - \beta$. First, we notice the asymmetry between $\alpha - \beta > 0$ and $\alpha - \beta < 0$ case which increases with $|\alpha - \beta|$. This is of course expected since the basement membrane breaks the symmetry by affecting the shape of a basally constricted cell more than the shape of an apically constricted cell. Second, the wavelength in the limit $\kappa \to 0$ is finite and seems to depend very little on $\alpha - \beta$ [Fig. 5(c)]. In this regime, the basement membrane curvature is very large and therefore modeling the membrane elasticity using the linear theory is not justified. As discussed above, the $\kappa \to 0$ limit can be interpreted as the absence of the membrane where the optimal wavelength is

determined by the constraint that the lengths of cell sides be positive and is of the order of $2l_0 \approx 2\sqrt{\alpha+\beta}$.

IV. DISCUSSION

Usually, the cell base is an isometric polygon, its size being of the same order of magnitude as the cell height [Fig. 1(a)]. Thus, none of the surface energy contributions can be neglected and certain 3D effects left out in the simplified 2D model should be accounted for in our continuum theory. Following the same steps as in the reduced-dimensionality case, we derive the full 3D Lagrangian for longitudinal folds which reads

$$\mathcal{L}^{3D} = (\alpha+\beta)r + \frac{\alpha-\beta}{2} r\dot{\psi} l + l + r^2 l^2 + \frac{1}{8}\dot{\psi}^2 + \mu r l + \gamma(s)(\dot{x} - \cos\psi) + \eta(s)(\dot{y} + \sin\psi) + \xi\dot{r}. \tag{12}$$

Here r, $1/c$, and l are measured in units of $\sqrt[3]{V_c}$, where V_c is the effective cell volume. The Lagrange multiplier ξ has been introduced to enforce the cylindrical symmetry ($r = \text{const}$) [26]. If this result is viewed as a function of c and l alone, the moduli of the different terms depend on r as opposed to the 2D case where the whole energy functional is simply rescaled by r. Additionally, the surface energy of cell sides which are perpendicular to the folds [the front and the rear cell sides in Fig. 1(a)] is here expressed as a linear term in tissue thickness. However, this is not expected to lead to a qualitative difference compared to the 2D mechanics since the linear term in l only adds to the Lagrange multiplier for the fixed volume constraint $\int_0^S lr\,ds = V$.

It can be shown that $\psi(s)$ obeys the same differential equation as in the 2D case [Eq. (5)]. Yet 3D effects do appear in thickness modulation which is here inversely proportional to the equilibrium cell depth $r = \sqrt{V/[(\alpha+\beta)S]}$,

$$l^{3D}(s) = l_0^{3D} - \frac{\alpha-\beta}{4r}\dot{\psi}(s), \tag{13}$$

where $l_0^{3D} = V/(rS)$ [in zero-order approximation in the differential tension $l_0^{3D} \approx (\alpha+\beta)^{2/3}$ and $r \approx (\alpha+\beta)^{-1/3}$]. They also enter the boundary condition for $\dot{\psi}(S)$, which reads $\dot{\psi}(S) = \pm 8\sqrt{(\alpha+\beta)r - (V/S)^2 - \gamma}/\sqrt{2-(\alpha-\beta)^2}$.

Taking into account the expression for tissue thickness [Eq. (13)], a simplified energy functional for the shape of the tissue cross-section midline that includes 3D effects is obtained: $dw^{3D}/ds = \text{const} + (k_e/2)(c-c_0)^2$, where $c_0 = 2(\alpha-\beta)/\{[2-(\alpha-\beta)^2]r\}$ is the tissue spontaneous curvature. Here, however, the spontaneous curvature does not affect the equilibrium shape, since the integral of curvature over periodic curve in 2D plane is 0 [31], and thus the energy difference between the flat and the fold state again reads $w^{3D} - w_{\text{flat}}^{3D} = (k_e/2)\int_0^S c^2 ds$.

In the case of cylindrical epithelium studied here [26], the deformation in the plane perpendicular to the folds could induce stresses in the third dimension, i.e., along the folds. In particular, the deviation of $r = \sqrt{V/[(\alpha+\beta)S]}$, which is optimal on the scale of the whole waveform and is constant along it, from the locally optimal value $r_0 = \sqrt{c^2+8l}/(2\sqrt{2}l)$ at fixed c and l can be viewed as a measure for the local stress in the zero-curvature direction:

$$\sigma_{\text{loc}} = \sigma_0\left(\frac{r}{r_0} - 1\right), \tag{14}$$

where σ_0 is the magnitude of the stress. We can distinguish three regimes: (i) If $\sigma_{\text{loc}} = 0$, then there are no local stresses; (ii) if $\sigma_{\text{loc}} > 0$, then there is a tendency for compression; and (iii) if $\sigma_{\text{loc}} < 0$, then there is a tendency for expansion in the direction perpendicular to the cross section. These stresses could further induce deformations in the third dimension. For such processes a full 3D generalization of the theory is needed. Due to geometric reasons the mechanics described by such a theory is expected to differ considerably and could give rise to various epithelial morphologies such as villi, crypts, and zig-zag folds.

V. CONCLUSIONS

We derived a continuum theory explaining the elasticity of an epithelium built from dropletlike cells characterized by differential surface tensions of cell sides. We introduced tissue thickness, i.e., cell height, as a variable which together with the curvature describes the tissue shape. Thickness modulation resulting from the thickness-curvature coupling is not only the signature of the mechanics presented here but also is an essential mechanism needed for folded epithelia to be energetically preferred over flat epithelia. As shown here, spontaneous folding can be described simply by the bending elasticity with a negative bending modulus.

The thickness modulation has been until recently an overlooked feature of epithelial shapes [18]. In elastic models, it is usually associated with large deformations and is locally induced by a large curvature. For example, various elastic models of highly deformed tissues give results which show a considerable curvature dependence of the thickness along waveforms [11,12,15]. Similarly, within the Kirchoff-Love plate theory where the thickness is considered constant, a simple argument addressing the bending of an incompressible plate can be used to show that, to lowest order, the change in thickness due to the curvature $\Delta L = L^2C/4$. However, the curvature dependence of the thickness may not be related only to ordinary elastic materials. In our model the local thickness modulation depends on the local curvature as well, but it is additionally governed by the apicobasal differential tension. Interestingly, in the case of vanishing differential tension the thickness no longer depends on the curvature, at least not within the first-order approximation in $(c/2l)^2$ [Eq. (2)]. The next order gives a negligible thickness modulation $\Delta l \approx c^4/(128l_0^3)$. Thus, the thickness modulation here indeed results from the apicobasal polarity as an intrinsic property of the tissue.

An advantage of the approach presented here is that it allows one to understand and compare the mechanics of different models just by analyzing effective elasticity functionals before minimizing them. In Ref. [16] the epithelial cross section with a fixed enclosed area has been studied as a model of gastrulation in *Drosophila*. It has been shown that the nonconfined epithelium can form very simple shapes reminiscent of the shapes of 2D lipid vesicles [29] as long as $|\alpha-\beta| < \sqrt{2}$ as well as more complex shapes with multiple constrictions either

on the apical side or on the basal side of the tissue for $\alpha > \beta$ and $\alpha < \beta$, respectively (Fig. 3(a) in Ref. [16]). The continuum theory presented here helps us to understand this sensitivity to $|\alpha - \beta|$ since it shows that the conceptually different behavior is a consequence of epithelial bending modulus' dependence on apicobasal differential tension which can either promote or suppress spontaneous folding. We formally derive this in Appendix E. A similar model of 3D incompressible epithelial cells, where instead of surface tension apical cell sides are characterized by the apical belt line tension, has been studied in Ref. [19]. The continuum theory seems the most appropriate tool for the comparison of both models in terms of elasticity. We show in Appendix E that the elasticities of both model epithelia are qualitatively very similar. For the case of cylindrical symmetry they can be both reduced to Euler's elastica problem and the main signature of both is the thickness modulation that results from the apicobasal asymmetry.

Studying coarse-grained discrete models of epithelia in the continuum limit has several advantages. It contributes to the understanding of the underlying mechanics and it distinguishes between mechanisms for the formation of modulated epithelial morphologies. In this paper we showed that the elasticity of epithelia might not differ much from the elasticity of simpler systems such as flexible rods and plates, yet the internal forces due to subcellular mechanics can induce spontaneous buckling which is not the case with ordinary elastic materials.

ACKNOWLEDGMENTS

We thank Nick Štorgel, Ana Hočevar, Michael Kozlov, Jacques Prost, and Antonio Šiber for stimulating discussions. This work was supported by the Slovenian Research Agency (Grant No. P1-0055) and by the European Science Foundation Research Networking Programme QuanTissue.

APPENDIX A: LATERAL TENSION DENSITY

The energy of an infinitesimally small segment of tissue reads

$$dW = (\Gamma_a + \Gamma_b)\frac{dA}{L} + \frac{\Gamma_a - \Gamma_b}{2} C dA + \frac{d\Gamma_l}{dA} L dA. \quad \text{(A1)}$$

The energy of a tissue with a reference cross-section area A_c, a constant curvature C, and a thickness L can be then calculated by integrating Eq. (A1) and has to be equal to the energy of a single cell with the same cross-section area A_c:

$$\int_{A_c} \frac{\partial W}{\partial A} dA = W_1. \quad \text{(A2)}$$

Here W_1 is the energy of a discrete cell

$$W_1 = (\Gamma_a + \Gamma_b)\frac{A_c}{L} + \frac{\Gamma_a - \Gamma_b}{2} C A_c + \Gamma_l L \sqrt{1 + \left(\frac{C A_c}{2L}\right)^2}. \quad \text{(A3)}$$

The lateral tension density can be expressed from Eq. (A2) and is given by

$$\frac{d\Gamma_l}{dA} = \frac{\Gamma_l}{A_c}\sqrt{1 + \left(\frac{C A_c}{2L}\right)^2}. \quad \text{(A4)}$$

The energy per unit length in nondimensional form then reads

$$\frac{dw}{ds} = \alpha + \beta + \frac{\alpha - \beta}{2} lc + l^2 \sqrt{1 + \left(\frac{c}{2l}\right)^2}, \quad \text{(A5)}$$

where the length scale is $\sqrt{A_c}$ and the energy scale is $\Gamma_l \sqrt{A_c}$. In the columnar epithelium cells are tall, and thus $(c/2l)^2 \ll 1$ so the energy functional can be expanded as

$$\frac{dw}{ds} \approx \alpha + \beta + \frac{\alpha - \beta}{2} lc + l^2 + \frac{1}{8} c^2. \quad \text{(A6)}$$

APPENDIX B: EULER-LAGRANGE EQUATIONS

It is convenient to write the Lagrangian $\mathcal{L}$ in $[\psi(s), l(s)]$ parametrization, where $\psi(s)$ is an angle between the tangent to the tissue midline and the horizontal axis. As before $\dot{x} = \cos\psi(s)$, $\dot{y} = -\sin\psi(s)$, so the Lagrangian reads

$$\mathcal{L} = \alpha + \beta + \frac{\alpha - \beta}{2}\dot{\psi} l + l^2 + \frac{1}{8}\dot{\psi}^2 + \mu l + \gamma(s)(\dot{x} - \cos\psi) + \eta(s)(\dot{y} + \sin\psi), \quad \text{(B1)}$$

where μ, $\gamma(s)$, and $\eta(s)$ are Lagrange multipliers. This yields the Euler-Lagrange equations for ψ and l:

$$\dot{\psi} = -\frac{2}{\alpha - \beta}(\mu + 2l), \quad \text{(B2a)}$$

$$\dot{l} = \frac{2(\alpha - \beta)}{(\alpha - \beta)^2 - 2}(\gamma \sin\psi + \eta\cos\psi). \quad \text{(B2b)}$$

Additionally, it turns out that all Lagrange multipliers are constant ($\dot{\gamma} = 0, \dot{\eta} = 0, \dot{\mu} = 0$) and that the constraint of fixed area of tissue cross section A_e can be taken into account by adding another differential equation $\dot{A}_e = l$. The boundary conditions read $\psi(0) = 0$, $x(0) = 0$, $y(0) = 0$, $A_e(0) = 0$, $\psi(S) = 0$, $x(S) = \lambda$, $y(S) = 0$, and $A_e(S) = A$.

The boundary-value problem can be further simplified by considering two boundary conditions. First, the periodic boundary condition $l(0) = l(S)$ can be recast as $l(S) - l(0) = \int_0^S \dot{l} ds = 0$. It follows $\eta[x(S) - x(0)] - \gamma[y(S) - y(0)] = 0$. Thus

$$\eta = 0\,. \quad \text{(B3)}$$

Similarly, the periodic boundary condition $\psi(0) = \psi(S)$ can be recast as $\psi(S) - \psi(0) = \int_0^S \dot{\psi} ds = 0$. It follows that $\mu S + 2A_e(S) = 0$. Thus

$$\mu = -\frac{2A}{S}. \quad \text{(B4)}$$

The Euler-Lagrange equation for ψ can now be decoupled from the Euler-Lagrange equation for l and the simplified system reads

$$\ddot{\psi} + \frac{8\gamma}{(\alpha - \beta)^2 - 2}\sin\psi = 0, \quad \text{(B5a)}$$

$$l = \frac{A}{S} - \frac{\alpha - \beta}{4}\dot{\psi}. \quad \text{(B5b)}$$

Note that in the case of $\alpha = \beta$ the system reduces to $\ddot{\psi} - 4\gamma \sin\psi = 0, l = A/S$.

The length of the integration interval S is derived by the minimization of the Hamiltonian $\mathcal{H}$ with respect to S:

$$\frac{d}{dS}\int_0^S \mathcal{H}(\psi,\dot{\psi},l)ds = \mathcal{H}(\psi,\dot{\psi},l)|_{s=S} = 0, \tag{B6}$$

where $\mathcal{H} = -\mathcal{L} + p_\psi\dot{\psi} + p_x\dot{x} + p_y\dot{y}$; $p_{q_i} = \partial\mathcal{L}/\partial\dot{q}_i$ are the conjugate momenta. The Hamiltonian reads

$$\mathcal{H} = \tfrac{1}{8}\dot{\psi}^2 - (\alpha+\beta) - l^2 - \mu l + \gamma\cos\psi, \tag{B7}$$

and an additional boundary condition for the curvature at $s = S$ is obtained:

$$\dot{\psi}(S) = \pm\frac{8}{2-(\alpha-\beta)^2}\sqrt{\alpha+\beta-\left(\frac{A}{S}\right)^2-\gamma}. \tag{B8}$$

APPENDIX C: THICKNESS MODULATION AT $\alpha - \beta = 0$

In order to study the tissue thickness modulation in the case of vanishing differential tension where the thickness-curvature coupling term $(\alpha-\beta)cl/2$ in Eq. (2) is zero, we need to go beyond the harmonic expansion of the surface tension model [Eq. (1)]. The lowest anharmonic term is $c^4/(128l^2)$ and in this approximation the Euler-Lagrange equation for thickness reads

$$l^4 = l^3\left(l_0 - \frac{\alpha-\beta}{4}\dot{\psi}\right) + \frac{1}{128}\dot{\psi}^4. \tag{C1}$$

An approximate analytical expression for thickness modulation can be obtained perturbatively. We write $l \approx [l_0 - (\alpha-\beta)\dot{\psi}/4] + \delta l$, where $|\delta l| \ll l_0 - (\alpha-\beta)\dot{\psi}/4$, and we insert this ansatz into Eq. (C1) which then gives

$$l \approx l_0 - \frac{\alpha-\beta}{4}\dot{\psi} + \frac{\dot{\psi}^4}{128[l_0-(\alpha-\beta)\dot{\psi}/4]^3}. \tag{C2}$$

In the case of zero differential tension ($\alpha-\beta=0$), Eq. (C2) simplifies to

$$l(s) = l_0 + \frac{\dot{\psi}(s)^4}{128l_0^3}. \tag{C3}$$

APPENDIX D: BASEMENT MEMBRANE

In the discrete representation the basement membrane energy can be written as $W_{\rm bm} = (K_{\rm bm}/2)C_{\rm bm}^2 L_b$, where $L_b = (1 - CL/2)\Delta A/L$ is the length of the basal cell side and the relationship between the midline curvature C and the curvature of the basement membrane $C_{\rm bm}$ reads $1/C_{\rm bm} = 1/C - L/2$. Thus, in the continuum limit ($\Delta A \to 0$) the dimensionless energy of the basement membrane reads

$$w_{\rm bm} = \frac{\kappa}{2}\int_0^S \frac{c^2}{1-lc/2}ds, \tag{D1}$$

where the nondimensional basement membrane bending modulus κ is measured in units of $\Gamma_l A_c$.

APPENDIX E: COMPARISON TO OTHER MODELS

First, we study an epithelial tube with fixed enclosed cross-section area. This system has been used as a model for the developing *Drosophila* embryo in Ref. [16]. During the gastrulation the tissue is invaginated on embryo's ventral side and forms the ventral furrow. In this model the interior of the embryo is filled with an incompressible fluid (yolk) which we model by an additional term in the Langragian $\nu x\sin\psi$, since $A_y = \int_0^S x\dot{y}ds = \int_0^S x\sin\psi ds = \text{const}$. Thus

$$\mathcal{L} = \alpha+\beta+\frac{\alpha-\beta}{2}\dot{\psi}l + l^2 + \frac{1}{8}\dot{\psi}^2 + \mu l + \nu x\sin\psi + \gamma(s)(\dot{x}-\cos\psi). \tag{E1}$$

The Euler-Lagrange equations for this case read $\dot{\psi} = -2(2l+\mu)/(\alpha-\beta)$, $\dot{l} = 2(\alpha-\beta)(\nu x\cos\psi + \gamma\sin\psi)/[(\alpha-\beta)^2-2]$, $\dot{x} = \cos\psi$, $\dot{\gamma} = \nu\sin\psi$, $\dot{A}_y = x\sin\psi$, $\dot{A}_e = l$, $\dot{\mu} = 0$, $\dot{\nu} = 0$ and have to satisfy the following boundary conditions: $\psi(0) = 0$, $x(0) = 0$, $A_y(0) = 0$, $A_e(0) = 0$, $\psi(S) = \pi$, $x(S) = 0$, $A_y(S) = A_y$, and $A_e(S) = A$.

Again, additional boundary conditions can be considered. First, the boundary condition $\psi(S) - \psi(0) = \pi$ gives $\mu = -2A_e(S)/S - \pi(\alpha-\beta)/(2S)$. In the case of shapes that are symmetric about both x and y axis also the condition $l(S) = l(0)$ holds true and gives $\gamma(0) = \gamma(S)$. The simplified Euler-Lagrange equations for ψ and l then read

$$\ddot{\psi} + \frac{8}{(\alpha-\beta)^2-2}(\nu x\cos\psi + \gamma\sin\psi) = 0, \tag{E2a}$$

$$l(s) = \frac{A}{S} - \frac{\alpha-\beta}{4}\left[\dot{\psi}(s) - \frac{\pi}{S}\right]. \tag{E2b}$$

The integration interval S has to be varied here as well. This is done in the same way as in the case of longitudinal folds [Eq. (B6)] by minimizing the Hamiltonian

$$\mathcal{H} = \tfrac{1}{8}\dot{\psi}^2 - (\alpha+\beta) - l^2 - \mu l - \nu x\sin\psi + \gamma\cos\psi. \tag{E3}$$

In Ref. [19] a 3D model of cells with a linear apical belt tension has been introduced. In this model the energy of a single cell reads

$$W = \Lambda_a p_a + \gamma_b A_b - \alpha_l A_l, \tag{E4}$$

where p_a is perimeter of the apical belt, Λ_a is the apical belt tension, γ_b is the basal surface tension, and α_l is the lateral surface tension. Following a similar derivation as in our model (Appendix A) we obtain the effective elastic energy per unit length in the limit of columnar cells [$(c/2lr)^2 \ll 1$]:

$$\frac{dw}{ds} = \alpha + \beta r + \frac{\alpha-\beta r}{2}cl + (\alpha r^2 - 2)l - 2r^2l^2 - \frac{1}{4}c^2. \tag{E5}$$

Here $\alpha = 2\Lambda_a/(\alpha_l\sqrt[3]{V_r})$ and $\beta = \gamma_b/\alpha_l$; s, l, r, and $1/c$ are measured in units of $\sqrt[3]{V_r}$ and w is measured in units of $\alpha_l V_r^{1/3}$. The result is qualitatively the same as in the model presented in the main text [Eq. (12)].

The authors of Ref. [19] have also included two additional energy terms accounting for the deformation of the nucleus, which were not considered when deriving Eq. (E5).

[1] L. D. Landau and E. M. Lifshitz, *Theory of Elasticity* (Pergamon Press, Oxford, 1986).

[2] https://math.dartmouth.edu/~euler/pages/E065.html.

[3] L. Pocivavsek, R. Dellsy, A. Kern, S. Johnson, B. Lin, K. Y. C. Lee, and E. Cerda, Science **320**, 912 (2008).

[4] H. Diamant and T. A. Witten, Phys. Rev. Lett. **107**, 164302 (2011).

[5] F. Brau, H. Vandeparre, A. Sabbah, C. Poulard, A. Boudaoud, and P. Damman, Nat. Phys. **7**, 56 (2011).

[6] Q. Wang and X. Zhao, Sci. Rep. **5**, 8887 (2015).

[7] F. Brau, P. Damman, H. Diamant, and T. A. Witten, Soft Matter **9**, 8177 (2013).

[8] Y. Klein, E. Efrati, and E. Sharon, Science **315**, 1116 (2007).

[9] H. Liang and L. Mahadevan, Proc. Natl. Acad. Sci. USA **106**, 22049 (2009).

[10] E. Cerda and L. Mahadevan, Phys. Rev. Lett. **90**, 074302 (2003).

[11] S. Budday, C. Raybaud, and E. Kuhl, Sci. Rep. **4**, 5644 (2014).

[12] T. Tallinen, J. Y. Chung, J. S. Biggins, and L. Mahadevan, Proc. Natl. Acad. Sci. USA **111**, 12667 (2014).

[13] E. Hannezo, J. Prost, and J. F. Joanny, Phys. Rev. Lett. **107**, 078104 (2011).

[14] M. Ben Amar and F. Jia, Proc. Natl. Acad. Sci. USA **110**, 10525 (2013).

[15] A. E. Shyer, T. Tallinen, N. L. Nerurkar, Z. Wei, E. S. Gil, D. L. Kaplan, C. J. Tabin, and L. Mahadevan, Science **342**, 212 (2013).

[16] A. Hočevar Brezavšček, M. Rauzi, M. Leptin, and P. Ziherl, Biophys. J. **103**, 1069 (2012).

[17] M. Krajnc, N. Štorgel, A. Hočevar Brezavšček, and P. Ziherl, Soft Matter **9**, 8368 (2013).

[18] N. Štorgel, M. Krajnc, P. Mrak, J. Štrus, and P. Ziherl (unpublished).

[19] E. Hannezo, J. Prost, and J. F. Joanny, Proc. Natl. Acad. Sci. USA **111**, 27 (2014).

[20] M. S. Steinberg, Science **141**, 401 (1963).

[21] N. Murisic, V. Hakim, I. G. Kevrekidis, S. Y. Shvartsman, and B. Audoly, Biophys. J. **109**, 154 (2015).

[22] R. Farhadifar, J.-C. Röper, B. Aigouy, S. Eaton, and F. Jülicher, Curr. Biol. **17**, 2095 (2007).

[23] A. Hočevar and P. Ziherl, Phys. Rev. E **80**, 011904 (2009).

[24] J. Derganc, S. Svetina, and B. Žekš, J. Theor. Biol. **260**, 333 (2009).

[25] Generally, any of the three surface tensions could also be negative. The effective surface tension includes a positive term due to cortex tension and a negative term due to adhesion, and if the magnitude of the latter is large enough the surface tension may be negative. Within our model, this would lead to unstable cells which would be either infinitely tall (if $\Gamma_l < 0$) or infinitely short (if $\Gamma_a < 0$ or $\Gamma_b < 0$). The instability has been considered in Ref. [19] where it was curbed by two additional energy terms accounting for deformation energy of the nucleus.

[26] Here "cylindrical" is used in the broad sense, describing a ruled surface defined by a single-parameter family of parallel lines. In this case, Gaussian curvature is zero and the shape is described by a single principal curvature.

[27] The equilibrium shape of flexible rod with bending rigidity K_b uniaxially compressed by the force F_x is the solution of Euler's Elastica equation $\ddot{\psi} - (F_x/K_b)\sin\psi = 0$.

[28] T. J. W. Wagner and D. Vella, Soft Matter **9**, 1025 (2013).

[29] U. Seifert, Phys. Rev. A **43**, 6803 (1991).

[30] A. Hočevar and P. Ziherl, Phys. Rev. E **83**, 041917 (2011).

[31] For closed curves in a plane the Gauss-Bonnet theorem states that $\oint c\,ds = 2\pi$ and reduces to $\int c\,ds = 0$ for nonclosed periodic curves.